# Crossover from a Molecular Bose-Einstein Condensate to a Degenerate Fermi Gas

M. Bartenstein,[1] A. Altmeyer,[1] S. Riedl,[1] S. Jochim,[1] C. Chin,[1] J. Hecker Denschlag,[1] and R. Grimm[1,2]

[1]*Institut für Experimentalphysik, Universität Innsbruck, Technikerstraße 25, 6020 Innsbruck, Austria*

[2]*Institut für Quantenoptik und Quanteninformation, Österreichische Akademie der Wissenschaften, 6020 Innsbruck, Austria*

(Received 8 January 2004; revised manuscript received 2 February 2004; published 23 March 2004)

We demonstrate a reversible conversion of a $^6Li_2$ molecular Bose-Einstein condensate to a degenerate Fermi gas of atoms by adiabatically crossing a Feshbach resonance. By optical *in situ* imaging, we observe a smooth change of the cloud size in the crossover regime. On the Feshbach resonance, the ensemble is strongly interacting and the measured cloud size is 75(7)% of the one of a noninteracting zero-temperature Fermi gas. The high condensate fraction of more than 90% and the adiabatic crossover suggest our Fermi gas to be cold enough to form a superfluid.

DOI: 10.1103/PhysRevLett.92.120401 PACS numbers: 03.75.Mn, 05.30.Fk, 32.80.Pj, 34.50.–s

Bose-Einstein condensation (BEC) of molecules formed by fermionic atoms was recently demonstrated [1–4]. The tunability of interactions in such systems provides a unique possibility to explore the Bose-Einstein condensate to Bardeen-Cooper-Schrieffer (BEC-BCS) crossover [5], an intriguing interplay between the superfluidity of bosons and Cooper pairing of fermions. While the BEC and BCS limits are both well understood, the crossover takes place in a strongly interacting regime, which represents a challenge for many-body theory.

Feshbach resonances [6] play a central role to control two-body interaction and have been used for conversion between fermionic atoms and bosonic molecules [7–10]. They are also the experimental key to investigate phenomena related to the BEC-BCS crossover. For example, it has been predicted in Ref. [11] that a pure molecular BEC can be converted into a superfluid Fermi gas by an adiabatic passage over the Feshbach resonance. Moreover, in the crossover regime where the interactions are unitarity limited, a universal behavior is expected [12,13]. Ultracold gases in that regime may provide new insights into other strongly interacting systems such as high-$T_c$ superconductors, $^3$He superfluids, and neutron stars.

A spin mixture of $^6$Li atoms in the lowest two hyperfine sublevels is an excellent system to investigate the crossover [14,15] based on a broad Feshbach resonance at a magnetic field of $B = 850$ G [16–18]. An efficient formation of ultracold molecules has been realized by three-body recombination [10,19], or by sweeping the magnetic field across the resonance [8]. The long lifetime of the molecules permits efficient evaporation [1,8,10] and facilitates slow, adiabatic changes of the system.

In this work, we explore the regime where the BEC-BCS crossover is expected by analyzing the density profiles of the trapped cloud at different magnetic fields. Our experimental setup is described in Ref. [1]. We load $2 \times 10^6$ precooled $^6$Li atoms into a single focused-beam dipole trap, which is generated by a 10 W Yb:YAG laser operating at a wavelength of 1030 nm. We evaporatively cool the cloud by exponentially lowering the trap depth with a time constant of 460 ms. The radial and axial trap frequencies are $\omega_r/2\pi = 110\ \mathrm{Hz}(P/\mathrm{mW})^{1/2}$ and $\omega_z/2\pi = (600B/\mathrm{kG} + 0.94P/\mathrm{mW})^{1/2}$ Hz, respectively, where $P$ is the laser power. The curvature of the magnetic field that we use for Feshbach tuning results in a magnetic contribution to the axial trapping. In the low power range where the molecular BEC is formed ($P < 50$ mW), the axial confinement is predominantly magnetic. During the whole evaporation process, the magnetic field is kept at $B = 764$ G. At this field the molecular binding energy is $\sim k_B \times 2\ \mu$K, where $k_B$ is Boltzmann's constant. For the scattering length of elastic molecule-molecule collisions, we expect $a_{\mathrm{mol}} = 2200a_0$, based on the predicted relation of $a_{\mathrm{mol}} = 0.6a$ [20] and an atomic scattering length of $a = 3500a_0$ [17]. Here $a_0$ is Bohr's radius. Using radio-frequency spectroscopy which allows us to distinguish signals from atoms and molecules [7], we observe a complete atom to molecule conversion when the thermal energy of the particles is reduced to values well below the molecular binding energy.

For detection we apply *in situ* absorption imaging to record spatial density profiles of the trapped ensemble. To image at high magnetic fields, we illuminate the cloud for 20 $\mu$s with a probe beam (intensity 0.5 mW/cm$^2$) tuned to the atomic $|2S_{1/2}, m_J = -1/2, m_I = 0\rangle \rightarrow |2P_{3/2}, m_J' = -3/2, m_I' = 0\rangle$ transition. The probe beam dissociates the molecules and is used to image the resulting atom cloud [3]. Compared to the absorption imaging of unbound atoms, we found that the detection efficiency of the molecules approaches 100% at fields higher than 750 G and $\sim$50% at 650 G. The difference is due to the Franck-Condon wave function overlap, which favors fields closer to the resonance where the interatomic separation in the molecular state is larger. In our cigar-shaped trap, the radial cloud size is on the order of our imaging resolution of 10 $\mu$m, while the axial cloud size of typically $\sim$100 $\mu$m can be accurately measured. We therefore obtain axial density distributions from images integrated radially.

  

To measure the condensate fraction, we adiabatically reduce the magnetic field from 764 to 676 G in a 200-ms linear ramp after completion of the evaporation ramp. This reduces the scattering length $a_{\mathrm{mol}}$ and thus increases the visibility of the characteristic bimodal distribution. Figure 1(a) shows a bimodal profile observed in this way with $N_{\mathrm{mol}} = N/2 = 4 \times 10^5$ molecules remaining at a final evaporation ramp power of 28 mW. A Gaussian fit to the thermal wings (dashed line) yields a temperature of $T = 430$ nK, which is a factor of 7.5 below the calculated trap depth of 3.2 $\mu$K. The observed condensate fraction of $\sim$20% is consistent with $1 - (T/T_c)^3$, where $T_c = 0.8 k_B^{-1} \hbar \bar{\omega} (N_{\mathrm{mol}}/1.202)^{1/3} = 500$ nK is the critical temperature, $\bar{\omega} = (\omega_r^2 \omega_z)^{1/3}$ is the mean vibration frequency, and the factor of 0.8 takes into account the $\sim$20% downshift in $T_c$ due to interactions [21].

We obtain pure molecular condensates when we continue the evaporation process down to final power levels of a few mW. Figure 1(b) shows an essentially pure condensate of $N_{\mathrm{mol}} = 2.0 \times 10^5$ molecules obtained at a final power of 3.8 mW, where the trap depth is 450 nK. The density profile is well fit by a Thomas-Fermi density distribution $\propto (1 - z^2/z_{\mathrm{TF}}^2)^2$ with a radius $z_{\mathrm{TF}} = 105$ $\mu$m. The corresponding peak molecular density is $1.2 \times 10^{13}$ cm$^{-3}$. In the image a thermal component is not discernable. A careful analysis of the profile provides us with a lower bound of 90% for the condensate fraction. For the chemical potential of the BEC, we obtain $\mu = \frac{1}{2} m_{\mathrm{mol}} \omega_z^2 z_{\mathrm{TF}}^2 = k_B \times 130$ nK. Here $m_{\mathrm{mol}} = 2m$ is the mass of the $^6$Li dimer. Based on the prediction $a_{\mathrm{mol}} = 0.6a = 650a_0$, the calculated chemical potential of $\frac{1}{2}(15\hbar^2 N_{\mathrm{mol}} \bar{\omega}^3 a_{\mathrm{mol}} \sqrt{m_{\mathrm{mol}}})^{2/5} = k_B \times 155$ nK is consistent

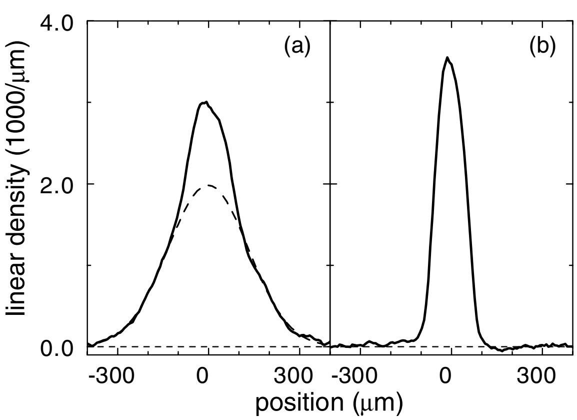


FIG. 1. Axial density profiles of a partially condensed (a) and fully condensed (b) molecular cloud. The profiles are derived from averaging seven *in situ* images taken at a magnetic field of $B = 676$ G after evaporation at the production field of 764 G. (a) When the evaporation ramp is stopped with $4 \times 10^5$ molecules at a final laser power of 28 mW, a characteristic bimodal distribution is observed with a condensate fraction of $\sim$20%. The dashed curve shows Gaussian fit to the thermal fraction. (b) At a final laser power of 3.8 mW, an essentially pure condensate of $2 \times 10^5$ molecules is obtained.

with the observed value of $k_B \times 130$ nK considering the experimental uncertainty. In particular, the particle number is calibrated to within a factor of 1.5 through fluorescence imaging [10].

The pure molecular BEC at 764 G serves as our starting point for exploring the crossover to the degenerate Fermi gas. Before we change the magnetic field, we first adiabatically increase the trap power from 3.8 to 35 mW in a 200-ms exponential ramp. The higher power provides a trap depth of $\sim k_B \times 2$ $\mu$K for the atoms, which is roughly a factor of 2 above the Fermi energy, and avoids spilling of the Fermi gas produced at magnetic fields above the resonance [1]. The compression increases the peak density of the condensate by a factor of 2.5. All further experiments reported here are performed in the recompressed trap with $\omega_r/2\pi = 640$ Hz and $\omega_z/2\pi = (600B/\mathrm{kG} + 32)^{1/2}$ Hz.

We measure the lifetime of the BEC in the compressed trap at 764 G to be 40 s. The peak molecular density is estimated to be $n_{\mathrm{mol}} = (15/8\pi)(\omega_r/\omega_z)^2 N_{\mathrm{mol}}/z_{\mathrm{TF}}^3 = 1.0(5) \times 10^{13}$ cm$^{-3}$. This provides an upper bound for the binary loss coefficient of $1 \times 10^{-14}$ cm$^3$/s, and is consistent with previous measurements in thermal molecular gases [8,10] together with the predicted scattering length scaling [20] and the factor-of-2 suppression of binary collision loss in a condensate.

For exploring the crossover to a Fermi gas we apply slow magnetic-field ramps. To ensure their adiabaticity, we performed several test experiments. In one series of measurements we ramped up the field from 764 to 882 G and back to 764 G with variable ramp speed. This converts the molecular BEC into a strongly interacting Fermi gas and vice versa. Therefore substantial changes are expected in the cloud size. After the up-and-down ramp, we observe an axial oscillation of the ensemble at the quadrupolar excitation frequency [1,22]. This collective oscillation is the lowest excitation mode of the system and is thus sensitive to nonadiabaticity effects. We observe axial oscillations with relative amplitudes of $>$ 5% for ramp speeds above 1.2 G/ms. For ramp speeds of 0.6 G/ms and lower, the axial oscillation was no longer visible.

We also checked the reversibility of the crossover process by linearly ramping up the magnetic field from 764 to 1176 G and down again to 764 G within 2 s (ramp speed of $\pm$0.41 G/ms). In Fig. 2, we compare the axial profile taken after this ramp (●) with the corresponding profile obtained after 2 s at fixed magnetic field (○). The comparison does not show any significant deviation. This highlights that the conversion into a Fermi gas and its back-conversion into a molecular BEC are lossless and proceed without noticeable increase of the entropy.

To investigate the spatial profile of the trapped gas in different regimes, we start with the molecular BEC at 764 G and change the magnetic field in 1-s linear ramps to final values between 740 and 1440 G. Images are then taken at the final ramp field. To characterize the size of

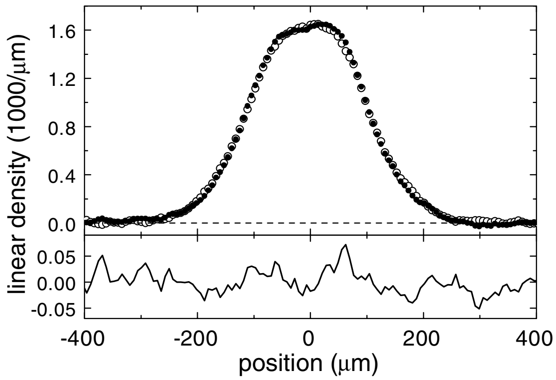


FIG. 2. Axial profile of a molecular BEC at 764 G (●) after its conversion into a Fermi gas at 1176 G and subsequent back conversion. Two 1-s magnetic field ramps are applied in this reversible process. For reference we show the corresponding profile observed without the magnetic field ramp (○). The density profiles are obtained by averaging over 50 images. The difference shown in the lower graph is consistent with the drifts of a residual interference pattern in the images.

the trapped gas, we determine the root-mean-squared axial size $z_{\rm rms}$. This rms size is related to the axial radius $z_{\rm TF}$ by $z_{\rm rms} = z_{\rm TF}/\sqrt{7}$ in the case of a pure BEC in the Thomas-Fermi limit and by $z_{\rm rms} = z_{\rm TF}/\sqrt{8}$ in the cases of zero-temperature noninteracting or strongly interacting Fermi gases [23].

Figure 3(b) shows how the measured axial size $z_{\rm rms}$ changes with the magnetic field. For comparison, Fig. 3(a) displays the magnetic-field dependence of the atomic scattering length $a$. Up to 950 G, an increase in $z_{\rm rms}$ is due to the crossover from the molecular BEC to the degenerate Fermi gas. For higher magnetic fields, the axial cloud size of the Fermi gas shrinks with $B$ as the axial magnetic confinement increases ($\omega_z \propto \sqrt{B}$).

For the following discussions, we normalize the observed size to the one expected for a noninteracting Fermi gas. In particular, this removes the explicit trap dependence. In Fig. 3(c), we show the normalized axial size $\zeta = z_{\rm rms}/z_0$, where $z_0 = (E_F/4m\omega_z^2)^{1/2}$ is the rms axial size of a noninteracting zero-temperature Fermi gas with $N = 4 \times 10^5$ atoms. The Fermi energy $E_F = \hbar^2 k_F^2/2m = \hbar\bar{\omega}(3N)^{1/3}$ amounts to $k_B \times 1.1\ \mu$K at 850 G, and the Fermi wave number $k_F$ corresponds to a length scale of $k_F^{-1} = 3600 a_0$.

Below the Feshbach resonance, the observed dependence of the cloud size agrees well with the mean-field behavior of a BEC in the Thomas-Fermi limit. In this regime, the normalized size is given by $\zeta = 0.688(a_{\rm mol}/a)^{1/5}(E_F/E_b)^{1/10}$, where $E_b = \hbar^2/ma^2$ is the molecular binding energy. Figure 3(c) shows the corresponding curve (solid line) calculated with $a_{\rm mol}/a = 0.6$ [20]. This BEC limit provides a reasonable approximation up to $\sim$800 G; here the molecular gas interaction parameter is $n_{\rm mol}a_{\rm mol}^3 \approx 0.08$. Alternatively, the interaction strength can be expressed as $k_F a \approx 1.9$.

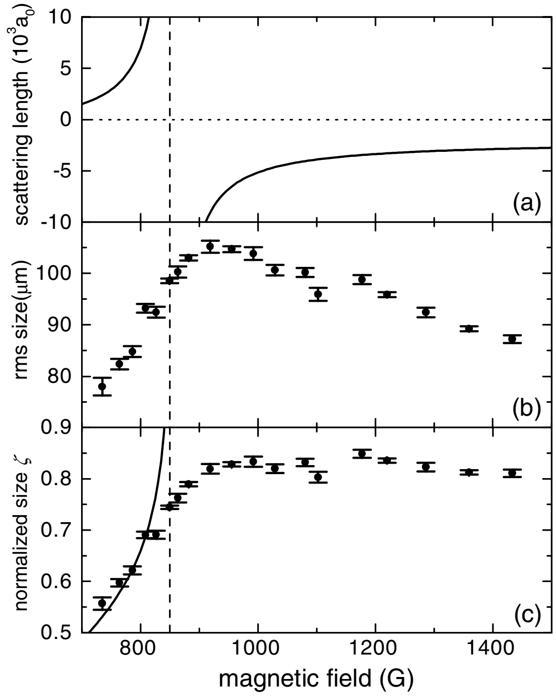


FIG. 3. Axial cloud size measurements across the Feshbach resonance. In (a) the atomic scattering length $a$ is shown according to [17]; the resonance at 850 G is marked by the vertical dashed line. The data in (b) display the measured rms cloud sizes. In (c), the same data are plotted after normalization to a noninteracting Fermi gas. The solid line shows the expectation from BEC mean-field theory with $a_{\rm mol} = 0.6a$. In (b) and (c), the error bars show the statistical error of the size measurements from typically five individual images.

The crossover to the Fermi gas is observed in the vicinity of the Feshbach resonance between 800 and 950 G; here $\zeta$ smoothly increases with the magnetic field until it levels off at 950 G, where the interaction strength is characterized by $k_F a \approx -1.9$. Our results suggest that the crossover occurs within the range of $-0.5 \lesssim (k_F a)^{-1} \lesssim 0.5$, which corresponds to the strongly interacting regime. The smoothness of the crossover is further illustrated in Fig. 4. Here the spatial profiles near the resonance show the gradually increasing cloud size without any noticeable new features.

On resonance a universal regime is realized [12–14], where scattering is fully governed by unitarity and the scattering length drops out of the description. Here the normalized cloud size can be written as $\zeta = (1 + \beta)^{1/4}$, where $\beta$ parametrizes the mean-field contribution to the chemical potential in terms of the local Fermi energy [14]. At 850 G our measured value of $\zeta = 0.75 \pm 0.07$ provides $\beta = -0.68^{+0.13}_{-0.10}$. Here the total error range includes all statistic and systematic uncertainties with the particle number giving the dominant contribution. Note that the uncertainty in the Feshbach resonance position is not included in the errors [18]. Our experimental results reveal a stronger interaction effect than previous measurements that yielded $\beta = -0.26(7)$ at $T = 0.15T_F$ [14]

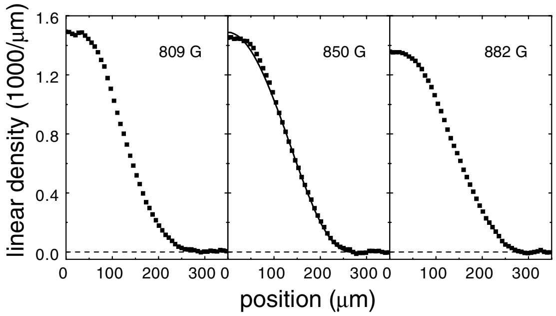


FIG. 4. Observed axial density profiles near the Feshbach resonance, averaged over 50 images and symmetrized to reduce imaging imperfections. The rms cloud sizes are 93, 99, and 103 $\mu$m at $B = 809$, 850, and 882 G, respectively. For comparison, the on-resonance data at 850 G are shown together with a fit by the expected profile $\propto (1 - z^2/z_{\rm TF}^2)^{5/2}$. The small deviation near the top is due to a residual interference pattern in the images.

and $\beta \approx -0.3$ at $T = 0.6T_F$ [15]. Our value of $\beta$ lies within the range of the theoretical predictions for a zero-temperature Fermi gas: $-0.67$ [12,24], $-0.43$ [24], and, in particular, $-0.56(1)$ from a recent quantum Monte Carlo calculation [25].

Beyond the Feshbach resonance, in the Fermi gas regime above 950 G, we observe an essentially constant normalized cloud size of $\zeta = 0.83 \pm 0.07$. In this regime, the interaction parameter $k_F a$ is calculated to vary between $-2$ (at 950 G) and $-0.8$ (at 1440 G), which allows us to estimate $\zeta$ to vary between 0.90 and 0.95 based on the interaction energy calculations in Ref. [12]. Our observed values are somewhat below this expectation, which requires further investigation.

In summary, we have demonstrated the smooth crossover from a molecular condensate of $^6$Li dimers to an atomic Fermi gas. Since the conversion is adiabatic and reversible, the temperature of the Fermi gas can be estimated from the conservation of entropy [11]. Our high condensate fraction of $> 90\%$ suggests a very small entropy which in the Fermi gas limit corresponds to an extremely low temperature of $k_B T < 0.04 E_F$. In this scenario, superfluidity can be expected to extend from the molecular BEC regime into the strongly interacting Fermi gas regime above the Feshbach resonance where $k_F a \lesssim -0.8$. Our experiment thus opens up intriguing possibilities to study atomic Cooper pairing and superfluidity in resonant quantum gases.

We thank G.V. Shlyapnikov, W. Zwerger, and S. Stringari and his group for very useful discussions. We acknowledge support by the Austrian Science Fund (FWF) within SFB 15 (project part 15) and by the European Union in the frame of the Cold Molecules TMR Network under Contract No. HPRN-CT-2002-00290. C. C. thanks the FWF for financial support.

[1] S. Jochim *et al.*, Science **302**, 2101 (2003); published online 13 November 2003 (www.sciencemag.org/cgi/content/abstract/1093280v1).
[2] M. Greiner, C. A. Regal, and D. S. Jin, Nature (London) **426**, 537 (2003).
[3] M. Zwierlein *et al.*, Phys. Rev. Lett. **91**, 250401 (2003).
[4] T. Bourdel *et al.*, cond-mat/0403091.
[5] A. J. Leggett, in *Modern Trends in the Theory of Condensed Matter*, edited by A. Pekalski and R. Przystawa (Springer-Verlag, Berlin, 1980); P. Nozières and S. Schmitt-Rink, J. Low Temp. Phys. **59**, 195 (1985); M. Drechsler and W. Zwerger, Ann. Phys. (Leipzig) **1**, 15 (1992); E. Timmermans, K. Furuya, P.W. Milonni, and A.K. Kerman, Phys. Lett. A **285**, 228 (2001); M. Holland, S..J. M. F. Kokkelmans, M. L. Chiofalo, and R. Walser, Phys. Rev. Lett. **87**, 120406 (2001); Y. Ohashi and A. Griffin, Phys. Rev. Lett. **89**, 130402 (2002); R. Combescot, Phys. Rev. Lett. **91**, 120401 (2003); A. Perali, P. Pieri, and G. C. Strinati, Phys. Rev. A **68**, 031601(R) (2003); J. Stajic *et al.*, cond-mat/0309329.
[6] E. Tiesinga, B. J. Verhaar, and H. T. C. Stoof, Phys. Rev. A **47**, 4114 (1993); S. Inouye *et al.*, Nature (London) **392**, 151 (1998).
[7] C. A. Regal, C. Ticknor, J. L. Bohn, and D. S. Jin, Nature (London) **424**, 47 (2003).
[8] J. Cubizolles *et al.*, Phys. Rev. Lett. **91**, 240401 (2003).
[9] K. E. Strecker, G. B. Partridge, and R. G. Hulet, Phys. Rev. Lett. **91**, 080406 (2003).
[10] S. Jochim *et al.*, Phys. Rev. Lett. **91**, 240402 (2003).
[11] L. D. Carr, G.V. Shlyapnikov, and Y. Castin, cond-mat/0308306.
[12] H. Heiselberg, Phys. Rev. A **63**, 043606 (2001).
[13] T.-L. Ho, Phys. Rev. Lett. **92**, 090402 (2004).
[14] K. M. O'Hara *et al.*, Science **298**, 2179 (2002); M. E. Gehm *et al.*, Phys. Rev. A **68**, 011401 (2003).
[15] T. Bourdel *et al.*, Phys. Rev. Lett. **91**, 020402 (2003).
[16] M. Houbiers, H. T. C. Stoof, W. McAlexander, and R. Hulet, Phys. Rev. A **57**, R1497 (1998).
[17] K. M. O'Hara *et al.*, Phys. Rev. A **66**, 041401(R) (2002).
[18] The resonance position is uncertain within a few 10 G.
[19] C. Chin and R. Grimm, cond-mat/0309078.
[20] D. S. Petrov, C. Salomon, and G.V. Shlyapnikov, cond-mat/0309010.
[21] S. Giorgini, L. P. Pitaevskii, and S. Stringari, Phys. Rev. A **54**, R4633 (1996).
[22] S. Stringari, Phys. Rev. Lett. **77**, 2360 (1996).
[23] We fit the density profiles with the function $\rho(z) = \rho_0(1 - z^2/z_{\rm r}^2)^\alpha$, where $\rho_0$, $z_r$, and $2 \leq \alpha \leq 2.5$ are free parameters. This function interpolates between the density profile of a pure BEC in the Thomas-Fermi limit with $\alpha = 2$ and a zero-temperature noninteracting or strongly interacting Fermi gas with $\alpha = 2.5$. The rms cloud size $z_{\rm rms}$ is obtained from $z_{\rm r}$ and $\alpha$ by $z_{\rm rms} = z_{\rm r}/\sqrt{3 + 2\alpha}$.
[24] G. A. Baker, Phys. Rev. C **60**, 054311 (1999).
[25] J. Carlson, S.-Y. Chang, V. R. Pandharipande, and K. E. Schmidt, Phys. Rev. Lett. **91**, 050401 (2003).